Interactions of High-Affinity Cationic Blockers with the Translocation Pores of *B. anthracis*, *C. botulinum*, and *C. perfringens* Binary Toxins

Sergey M. Bezrukov,[†*] Xian Liu,[§] Vladimir A. Karginov,[¶] Alexander N. Wein,[‡] Stephen H. Leppla,[‡] Michel R. Popoff,[||] Holger Barth,[**] and Ekaterina M. Nestorovich[§*]

[†]Program in Physical Biology, Eunice Kennedy Shriver National Institute of Child Health and Human Development and [‡]Microbial Pathogenesis Section, National Institute of Allergy and Infectious Diseases, National Institutes of Health, Bethesda, Maryland; [§]Department of Biology, The Catholic University of America, Washington, DC; [¶]Innovative Biologics, Herndon, Virginia; [||]Department of Host-Pathogen Interactions, Institut Pasteur, Paris, France; and [**]Institute of Pharmacology and Toxicology, University of Ulm Medical Center, Ulm, Germany

ABSTRACT Cationic β-cyclodextrin derivatives were recently introduced as highly effective, potentially universal blockers of three binary bacterial toxins: anthrax toxin of *Bacillus anthracis*, C2 toxin of *Clostridium botulinum*, and iota toxin of *Clostridium perfringens*. The binary toxins are made of two separate components: the enzymatic A component, which acts on certain intracellular targets, and the binding/translocation B component, which forms oligomeric channels in the target cell membrane. Here we studied the voltage and salt dependence of the rate constants of binding and dissociation reactions of two structurally different β-cyclodextrins (AmPrβCD and AMBnTβCD) in the PA_{63}, C2IIa, and Ib channels (B components of anthrax, C2, and iota toxins, respectively). With all three channels, the blocker carrying extra hydrophobic aromatic groups on the thio-alkyl linkers of positively charged amino groups, AMBnTβCD, demonstrated significantly stronger binding compared with AmPrβCD. This effect is seen as an increased residence time of the blocker in the channels, whereas the time between blockages characterizing the binding reaction on-rate stays practically unchanged. Surprisingly, the voltage sensitivity, expressed as a slope of the logarithm of the blocker residence time as a function of voltage, turned out to be practically the same for all six cases studied, suggesting structural similarities among the three channels. Also, the more-effective AMBnTβCD blocker shows weaker salt dependence of the binding and dissociation rate constants compared with AmPrβCD. By estimating the relative contributions of the applied transmembrane field, long-range Coulomb, and salt-concentration-independent, short-range forces, we found that the latter represent the leading interaction, which accounts for the high efficiency of blockage. In a search for the putative groups in the channel lumen that are responsible for the short-range forces, we performed measurements with the F427A mutant of PA_{63}, which lacks the functionally important phenylalanine clamp. We found that the on-rates of the blockage were virtually conserved, but the residence times and, correspondingly, the binding constants dropped by more than an order of magnitude, which also reduced the difference between the efficiencies of the two blockers.

INTRODUCTION

Several pathogenic species of *Bacillus* and *Clostridium* employ a unique and well-designed means of intoxicating eukaryotic cells—they secrete binary exotoxins that consist of two individual nonlinked proteins: an active/enzymatic (A) component and a binding/translocation (B) component (1–4). To gain access for their A components into the cytosol, the binary toxins rely on a similar cellular uptake mechanism. The B component of these toxins binds to a receptor on the surface of the target cells, self-assembles to form a ring-shaped oligomeric prepore that is able to bind the A components, and, after receptor-mediated endocytosis, is converted into an ion-conductive pore that mediates A component translocation from acidified endosomal vesicles into the cytosol.

With the exception of binary anthrax toxin, no extensive studies searching for effective therapies against the binary toxins have been reported. Remarkably, the binding/translocation B components are structurally conserved between the *Bacillus* and *Clostridium* families. They share a high level of amino acid homology and numerous functional similarities (2), whereas the enzymatic A components of these toxins are quite distinct and inhibit different normal cell functions. The similarities between the channel-forming B components suggest that these channels can be a specific universal target in the search for new, effective, broad-spectrum antitoxins against the *Bacillus* and *Clostridium* pathogenic species.

In this study we focus on three binary toxins: anthrax toxin of *Bacillus anthracis*, C2 toxin of *Clostridium botulinum*, and iota toxin of *C. perfringens*. After proteolytic activation, the truncated B components of these toxins (PA_{63}, C2IIa, and Ib) assemble into ring-shaped oligomers, the so-called prepores on the surface of eukaryotic cells or in solution. C2IIa and Ib prepores are heptamers (5), and PA_{63} was reported to form heptamers (6) as well as octamers (7). After the binding of A components, the cell-bound complexes are internalized by receptor-mediated endocytosis (8–16) and reach endosomal vesicles where the A components translocate across the endosomal membranes into the cytosol using the PA_{63}, C2IIa, and Ib pores as translocation corridors (5,16–21). In mildly acidic conditions, their B components form cation-selective oligomeric

Submitted March 5, 2012, and accepted for publication July 24, 2012.

*Correspondence: bezrukos@mail.nih.gov or nestorovich@cua.edu

Editor: Hagan Bayley.

0006-3495/12/09/1208/10 $2.00

http://dx.doi.org/10.1016/j.bpj.2012.07.050

channels in planar lipid membranes. The channel cationic selectivity decreases in the sequence PA_{63} > C2IIa > Ib (17,18,22,23). The mushroom-like (125-Å-diameter and 70-Å-long cap, and 100-Å-long stem) membrane-spanning $(PA_{63})_7$ pores were observed by negative-stain electron microscopy (24). With both the PA_{63} and C2IIa channels, the phenylalanine clamps (φ-clamps) F427 and F428, respectively, were found to catalyze the unfolding and translocation of the A component moieties across the membrane (25–29). The Phe at the corresponding position is also conserved in Ib (29), but the importance of the φ-clamp for the iota toxin transport is not clear as of yet.

One of the new promising inhibitory approaches involves obstructing the membrane pores with molecules having the same structural symmetry as the oligomeric pores (30–34). It was demonstrated that the tailor-made β-cyclodextrin derivatives carrying seven positively charged groups, 7+β-CD, efficiently blocked the PA_{63} pores in subnanomolar concentrations in vitro, and protected cultured macrophage-like cells and Fischer F344 rats against intoxication with lethal toxin (30,31) and DBA/2 mice against *B. anthracis* infection (35). Of most importance, we recently showed that AMBnTβCD efficiently protects cultured epithelial cells against intoxication with two clostridial binary toxins (C2 and iota) and blocks the ion current through C2IIa and Ib channels in planar lipid membranes (34).

The nature of the physical forces involved in 7+β-CD's interactions with the PA_{63}, C2IIa, and Ib channels remains unclear. On the basis of experiments with PA_{63}, we previously reported an order of magnitude increase in the inhibitory activity of seven positively charged aromatic hepta-6-alkylarylamine β-CD derivatives compared with their hepta-6-aminoalkyl analogs (31). Here, to study contributions of different forces to 7+β-CDs binding, we examine the basic features of PA_{63}, C2IIa, and Ib pore blockage by two structurally different derivatives: per-6-S-(3-amino)propylthio-β-cyclodextrin (AmPrβCD), and per-6-S-(3-aminomethyl)benzylthio-β-cyclodextrin (AMBnTβCD) (Fig. 1). AMBnTβCD differs from AmPrβCD by the aromatic rings inserted into alkyl chains carrying positively charged amino groups. To address the importance of the φ-clamp in the blockage, we also studied the F427A mutant of PA_{63} (25).

We start with a description of the static (average currents) and dynamic (noise power spectra) features of the single PA_{63}, C2IIa, Ib, and PA_{63} F427A channels reconstituted into planar lipid bilayers in blocker-free solutions, and proceed with the characterization of AmPrβCD and AMBnTβCD binding to these channels as a function of the applied transmembrane voltage and different KCl concentrations. In particular, we show that binding of both derivatives to the PA_{63} F427A mutant, quantified by the equilibrium binding constant, decreases by more than an order of magnitude, thus confirming the importance of the

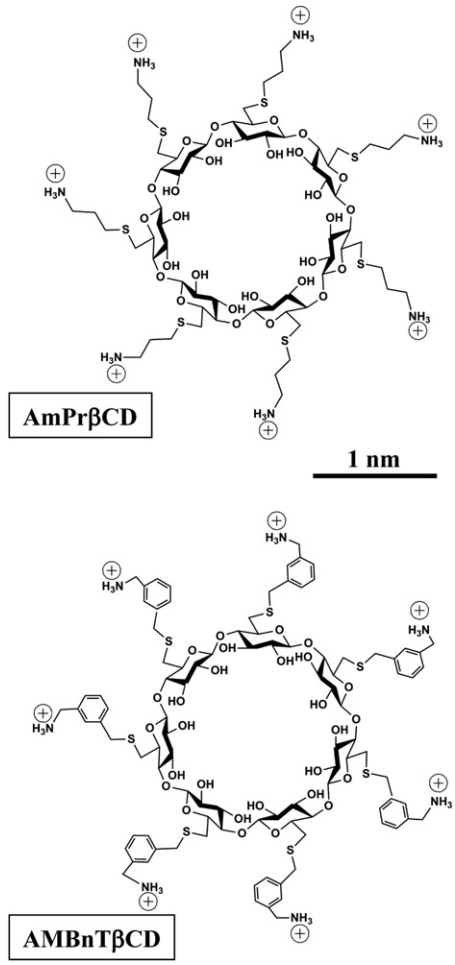

FIGURE 1 Two sevenfold symmetrical synthetic molecules, AmPrβCD (*top panel*) and AMBnTβCD (*bottom panel*) were used as blockers of the PA_{63}, C2IIa, and Ib pores.

φ-clamp for channel interaction with the blockers. Our main conclusion is that although both long-range Coulomb forces and interactions of the blocker charge with the transmembrane field are able to increase the residence time of the blocker in the channel by orders of magnitude, the leading interactions are related to salt-concentration-independent, short-range forces.

MATERIALS AND METHODS

Reagents

PA_{63} was purchased from List Biological Laboratories (Campbell, CA). The recombinant C2 toxin's C2IIa component and iota toxin's Ib component were prepared and activated as described previously (5,36,37). The F427A mutant of PA_{63} was created by Quick-Change mutagenesis of the pYS5 expression plasmid, and the protein was purified by procedures equivalent to those previously described (38). We used the following chemical reagents: KCl, MES, KOH, and HCl (Sigma-Aldrich, St. Louis, MO); purum hexadecane (Fluka, Buchs, Switzerland); diphytanoyl phosphatidylcholine (DPPC; Avanti Polar Lipids, Alabaster, AL); pentane (Burdick and Jackson, Muskegon, MI), and agarose (Bethesda Research Laboratory,

Gaithersburg, MD). Milli-Q water was used to prepare solutions. AMBnTβCD and AmPrβCD were custom synthesized at CycloLab (Budapest, Hungary) as described previously (31).

Channel reconstitution into planar lipid bilayers

To form solvent-free planar lipid bilayers using the lipid monolayer opposition technique (39), we employed a 5 mg/ml stock solution of DPPC in pentane. Bilayer lipid membranes were formed on a 60-80-μm diameter aperture in a 15-μm-thick Teflon film that separated the two compartments as described in detail elsewhere (33). The 0.1–2 M aqueous solutions of KCl were buffered at pH 6 (MES) at room temperature (23 $\pm$ 0.5)°C. Single channels were formed by adding 0.5 to 1 μl of 20 μg ml^{-1} solution of PA_{63} (wild-type (WT) and F427A mutant), (0.2–0.5) μl of 48 ng ml^{-1} solution of C2IIa, or (0.2–1) μl of 2.5 μg ml^{-1} solution of Ib to the 1.5 ml aqueous phase on the *cis* half of the chamber. For multichannel experiments, we applied ~1–2 μl of 0.2 mg ml^{-1} stock PA_{63}. Under this protocol, the channel insertions were always directional. The applied potential was defined as positive if it was higher on the side of protein addition.

RESULTS

PA_{63}, C2IIa, and Ib channels, but not the PA_{63} F427A channel, share 1/*f* current noise characteristics

Typical ion currents through the three single channels of PA_{63}, C2IIa, and Ib, reconstituted into planar lipid membranes in blocker-free 1 M KCl solutions, are presented in Fig. 2 *A*. The currents are shown at 1-ms resolution to illustrate the vigorous flickering of the channels between open and completely closed states. This type of fast flickering was reported previously (17,22,40,41) and recently discussed in more detail (33). The current through the channel formed by the F427A mutant of PA_{63} is shown in Fig. 2 *B*. The removal of the φ-clamp leads to a significant current increase, in agreement with earlier studies (25), and changes the channel dynamics. First, the F427A channel conductance does not flicker to a completely closed state. Second, the time hierarchy of the flickering is altogether different. As the current power spectra plotted in Fig. 3 against frequency f demonstrate, for all the WT PA_{63}, C2IIa, and Ib channels, the flickering is described by the complex non-Markov kinetics. The data in Fig. 3 were normalized by dividing the current power spectral density by the square of the mean current, and thus represent the relative fluctuation level to facilitate comparison of the dynamic properties of channels with different conductance. In similarity to our previous finding with PA_{63} (33), the power spectral density $S(f)$ of these relative current fluctuations was voltage independent (data not shown), suggesting that fluctuations in current i reflect equilibrium fluctuations in conductance g, $\delta i/\langle i\rangle = \delta g/\langle g\rangle$ (where quantities in brackets are averages). The 1/*f*-type shapes of the spectra for the WT channels, $S(f) \propto 1/f$, imply that the dynamics of their conformational transitions are characterized by a broad distribution of characteristic times that span many orders of magnitude. Interestingly, the current noise of the F427A mutant of PA_{63}, which lacks the functionally

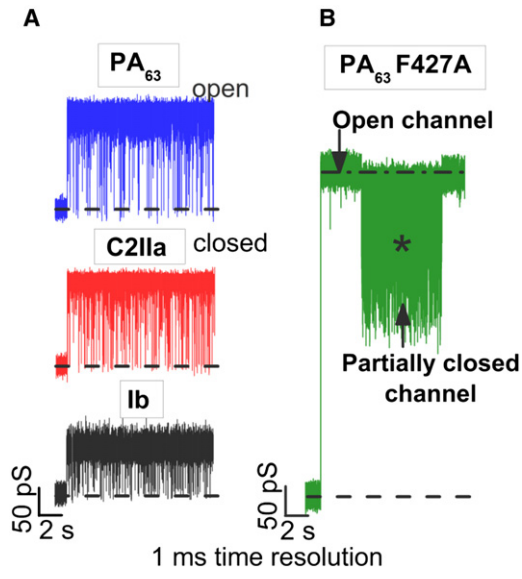

FIGURE 2 (*A*) In the absence of blockers, conductance of the PA_{63}, C2IIa, and Ib single channels reconstituted into planar lipid membranes demonstrate fast flickering between the open and closed states. (*B*) The F427A mutant of PA_{63} forms channels with much higher conductance and modified dynamics compared with those of the WT. Measurements were taken in 1 M KCl solutions at pH 6 buffered by 5 mM MES. The applied voltage for the data in panels *A* and *B* was 50 mV. The currents are given at 1-ms time resolution.

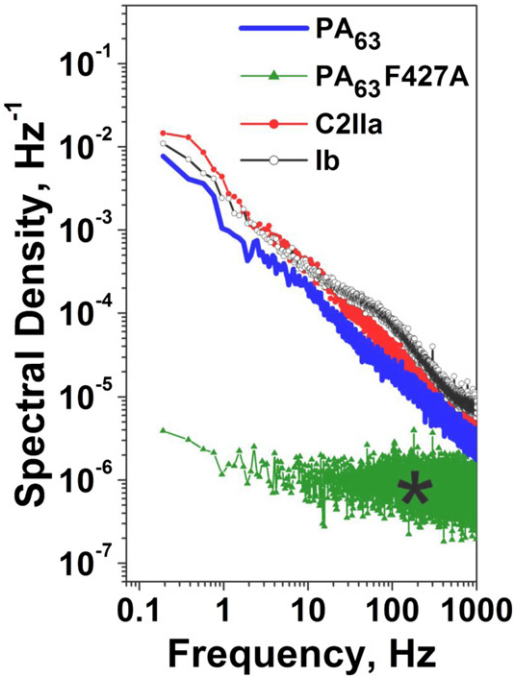

FIGURE 3 Power spectral densities of the normalized currents demonstrate a basic difference in the dynamic properties of the WT and the PA_{63} F427A mutant pores. The WT PA_{63}, C2IIa, and Ib single channels display an expressed 1/*f* behavior, whereas the mutant does not. The experimental conditions are the same as for Fig. 2.

important φ-clamp, is mostly devoid of this complex hierarchy of times even in the noisiest, partially closed states (Figs. 2 *B* and 3, marked with a *star*). The significance of these changed dynamics for the A component translocation remains to be clarified.

The spectra measured here for currents through WT single channels agree well with the results obtained earlier from multichannel membranes (40,42), thus demonstrating that the origin of the 1/*f* noise in the present systems is not related to channel-channel interactions. Rather, it is an inherent property of individual channels (43). In addition, PA_{63}, C2IIa, and Ib exhibited strong voltage-dependent gating (not shown) of an unknown origin that is observed with many β-barrel channels. This type of gating is highly asymmetrical (being more pronounced at *cis*-negative voltages) and decreases in the order PA_{63} > C2IIa >> Ib.

AmPrβCD- and AMBnTβCD-pore interactions

Fig. 4 *A* illustrates the effects of AmPrβCD and AMBnTβCD on the currents through the three WT channels. To show the effect more clearly, the time resolution of the current records in the figure was limited to 10 ms. Under this resolution, the 1/*f* fast flickering is filtered out to a significant extent. It can be seen that both blockers induce extra current interruptions in all three channels, with the lifetime in the blocked state (or blocker residence time) depending on the type of blocker molecule. Particularly, AMBnTβCD provides much longer current interruptions than its close analog AmPrβCD, which is missing aromatic rings on the linkers carrying positive charges (Fig. 1). The average times between successive current interruptions decrease with blocker concentration (30,33,34). Fig. 4 *B* shows that both blockers are significantly less potent with the F427A mutant of PA_{63}. The dwell times of the blockers in this channel are much shorter than in the WT PA_{63}. Please note the order-of-magnitude finer timescale in the figure and higher blocker concentration.

The blocker residence times are also strong functions of the applied voltage. The results presented in Fig. 5 were determined either by direct measurements and statistical analysis of the time distributions, which were single exponential (30,33,34), or by power spectral analysis of current fluctuations using the fitting by single Lorentzian spectra (33). Therefore, the PA_{63}, C2IIa, and Ib current fluctuations induced by AmPrβCD and AMBnTβCD could be described by a two-state Markov process. Fig. 5 demonstrates that for both blockers and all three WT channels, the blockage times are practically exponential in the voltage applied to the membrane. Although they differ consistently by the absolute value for the two blockers and for the three channels in the case of AmPrβCD, surprisingly, the slopes of the logarithm of the lifetimes versus voltage dependence are very close to each other, though somewhat lower for the less-efficient AmPrβCD ($d\lg\tau_{off}/dV = (13.9 \pm 0.3) \times 10^{-3}$ $(\mathrm{mV})^{-1}$) than for AMBnTβCD ($d\lg\tau_{off}/dV = (16.5 \pm 0.5) \times 10^{-3}$ $(\mathrm{mV})^{-1}$). In any case, all six systems can be characterized by the effective gating charge or apparent valence (44) of 1.1 ± 0.1 elementary charges.

The on- and off-rates of the blockage reaction were studied as functions of salt concentration. Fig. 6 shows

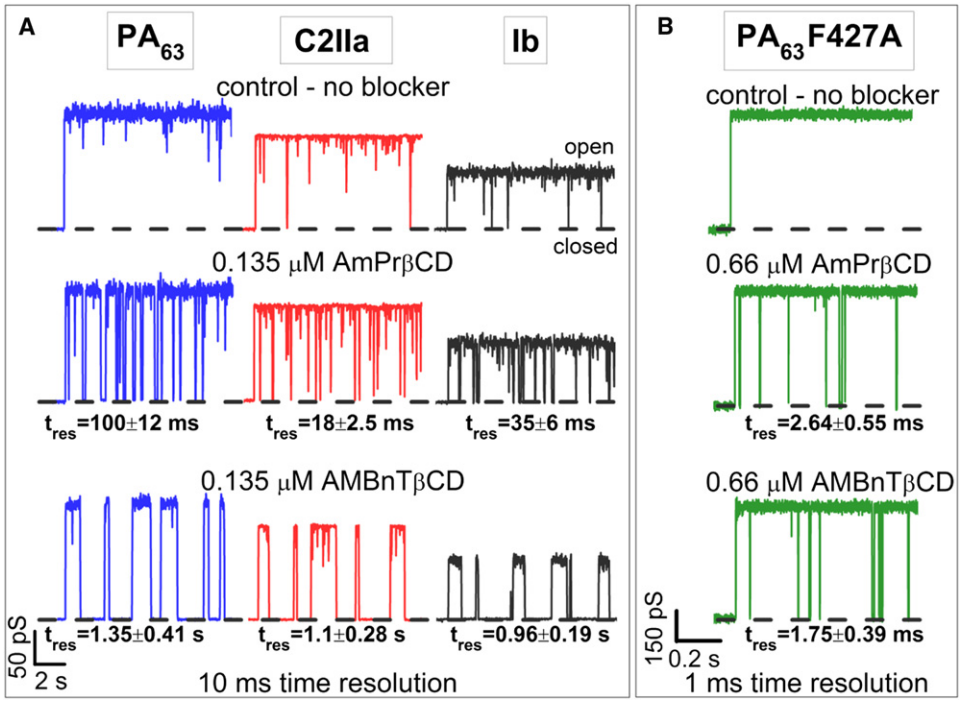

FIGURE 4 (*A*) Conductance of single PA_{63}, C2IIa, and Ib channels in the absence (*top*) and presence of 0.135 μM AmPrβCD (*middle row*) and AMBnTβCD (*bottom row*) blockers in the *cis* side of the chamber. Recordings are shown at 10-ms time resolution. AMBnTβCD displays a significantly longer binding lifetime with all channels compared with AmPrβCD, whereas the time between the blockage events, characterizing the on-rate of the binding reaction, seems to be practically unchanged. (*B*) The PA_{63} F427A mutant shows much shorter blockages for both AmPrβCD (*middle track*) and AMBnTβCD (*bottom track*) blockers. Recordings are shown at 1-ms time resolution. Other conditions for *A* and *B* are the same as for Fig. 2.

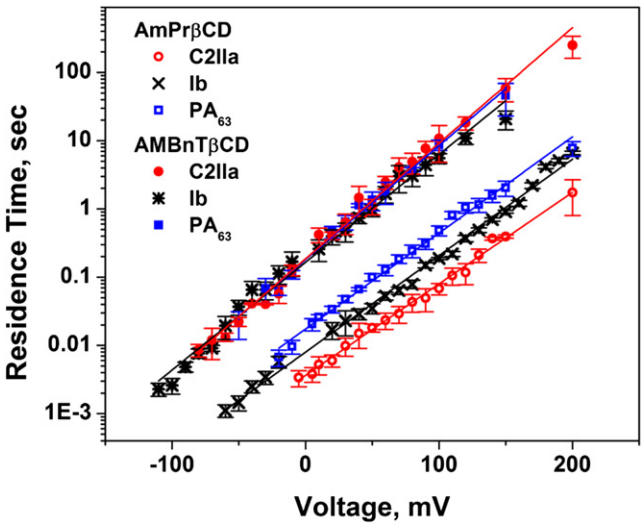

FIGURE 5 Residence times of blocker binding to the channels plotted as functions of transmembrane voltage reveal exponential voltage dependence. Membranes were bathed by 1 M KCl solution at pH 6. Blocker concentrations ranged from nanomolar to micromolar to ensure reliable statistics. Residence times were calculated from probability versus time histograms of the blockage events or by spectral analysis of current fluctuations as described previously (33). The solid lines through the data show single-exponential regression.

that for two different blockers with three different WT channels, a decrease in salt concentration leads to a substantial increase in the lifetimes, suggesting the involvement of long-range Coulomb interactions. However, the relative magnitude of the increase depends on the channel and

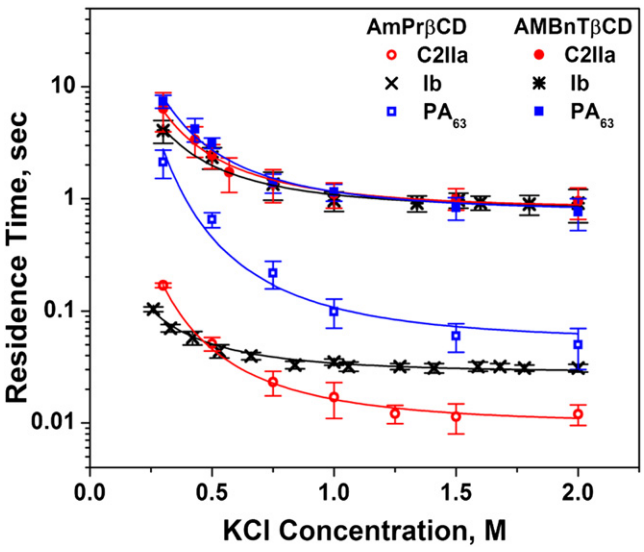

FIGURE 6 Residence times of blocker binding to the channels as functions of bulk salt concentration show different degrees of salt dependence for the three channels and two blockers. The salt dependence is most pronounced for AmPrβCD interacting with the PA_{63} pore. For the more-efficient AMBnTβCD, the dependence is weaker. The solid lines through the data are drawn according to Eqs. 3 and 4 with the fitting parameters given in the text. The applied voltage was +50 mV.

on the blocker. Interestingly, with the more-efficient AMBnTβCD, which carries extra hydrophobic aromatic groups (Fig. 1), the salt-dependent increase is much smaller than for AmPrβCD, especially in the case of the PA_{63} and C2IIa pores.

The on-rates of the blockage for AmPrβCD and AMBnTβCD are given in Table 1 for three voltages. It can be seen that the on-rates are quite comparable for all of the blocker/channel combinations studied. We also observed the on-rate decrease at increasing salt concentrations with AmPrβCD (data not shown, but see Nestorovich et al. (33)). The on-rate constant was calculated from the times between the successful blockages, τ_{on}, and blocker concentration in the bulk $[C^b_{\text{blocker}}]$ as $k_{on} = 1/(\tau_{on}[C^b_{\text{blocker}}])$. The data show a significant spread because we faced several challenges when determining the τ_{on} values. First, at the low blocker concentrations, there were indications of blocker sorption on the hydrophobic surfaces of the vials, syringes, pipette tips, and Teflon walls of the bilayer chamber. Second, under certain experimental conditions (e.g., at low voltages), the main difficulty with the direct τ_{on} determination was the need to separate the blockages from the fast flickering. The equal amplitudes of the current fluctuations for these two processes complicated the problem (see related discussions in Nestorovich et al. (33) and Blaustein et al. (41)). Third, the strong voltage gating of these channels at high transmembrane voltages, which in turn increases in the presence of the blocker (33), made the τ_{on} values at high voltages (>100 mV) statistically less reliable.

Table 2 compares the off-rates for the two blockers and all channels studied, including the F427A mutant of PA_{63} at 0.3 M KCl. It can be seen that removal of the φ-clamp increases the off-rates by more than an order of magnitude, which at the approximately conserved on-rates leads to a decreased efficiency of the blockers. This result correlates nicely with the multichannel measurements in Fig. 7, which

TABLE 1 Rate constants of binding reaction, k_{on}, for the two blockers and PA_{63} (WT and F427A mutant), C2IIa, and Ib channels measured at three different transmembrane voltages

	k_{on}, $(\text{Ms})^{-1}$		
	50 mV	100 mV	150 mV
	AmPrβCD		
PA_{63}	$(1.7 \pm 0.7) \times 10^7$	$(2.4 \pm 0.9) \times 10^7$	$(2.5 \pm 0.6) \times 10^7$
PA_{63} F427A	$(2.0 \pm 0.5) \times 10^7$	$(3.7 \pm 0.8) \times 10^7$	$(5.6 \pm 0.4) \times 10^7$
C2IIa	$(3.1 \pm 1.2) \times 10^7$	$(3.9 \pm 1.5) \times 10^7$	$(5.3 \pm 1.6) \times 10^7$
Ib	$(1.9 \pm 0.9) \times 10^7$	$(2.1 \pm 0.7) \times 10^7$	$(3.0 \pm 1.0) \times 10^7$
	AMBnTβCD		
PA_{63}	$(2.9 \pm 0.7) \times 10^7$	$(4.1 \pm 1.7) \times 10^7$	$(4.4 \pm 1.1) \times 10^7$
PA_{63} F427A	$(2.1 \pm 0.5) \times 10^7$	$(6.3 \pm 0.3) \times 10^7$	$(1.2 \pm 0.5) \times 10^8$
C2IIa	$(2.2 \pm 0.4) \times 10^7$	$(2.7 \pm 0.9) \times 10^7$	$(3.4 \pm 1.7) \times 10^7$
Ib	$(1.0 \pm 0.6) \times 10^7$	$(1.2 \pm 0.5) \times 10^7$	$(1.3 \pm 0.3) \times 10^7$

Data were obtained in 1 M KCl at pH 6 buffered by 5 mM MES.

TABLE 2 Rate constants of dissociation reaction, k_{off}, for the two blockers and PA_{63} (WT and F427A mutant), C2IIa, and Ib channels measured in 0.3 M KCl, at pH 6 at 50 mV applied voltage

	k_{off}, $(s)^{-1}$	
	AmPrβCD	AMBnTβCD
PA_{63}	0.47 ± 0.13	0.13 ± 0.02
PA_{63} F427A	10.8 ± 2.3	12.5 ± 2.3
C2IIa	5.9 ± 0.2	0.16 ± 0.06
Ib	11.9 ± 2.8	0.24 ± 0.06

show that the IC_{50} values characterizing PA_{63} F427A multichannel conductance inhibition by the two blockers are significantly higher and very close. Compared with its value for the WT PA_{63}, the AmPrβCD's IC_{50} increases 20 times (from 0.65 nM to 15 nM), whereas for the more effective AMBnTβCD the increase is more significant (~200-fold, from 0.14 nM to 25 nM).

DISCUSSION

One surprising observation of our study is related to the voltage dependence of the lifetimes in the blocked states (Fig. 5). Indeed, the slope of this dependence, which gives an apparent electrical distance (41,44–46) and is usually interpreted as the depth of blocker penetration in the channel, turns out to be practically the same for all six cases. They include two different blockers and three different channels that belong not only to three different species but also to two different families, *Bacillus* and *Clostridium*. This finding strongly suggests that the structural features responsible for blocker binding are remarkably similar among all three channels.

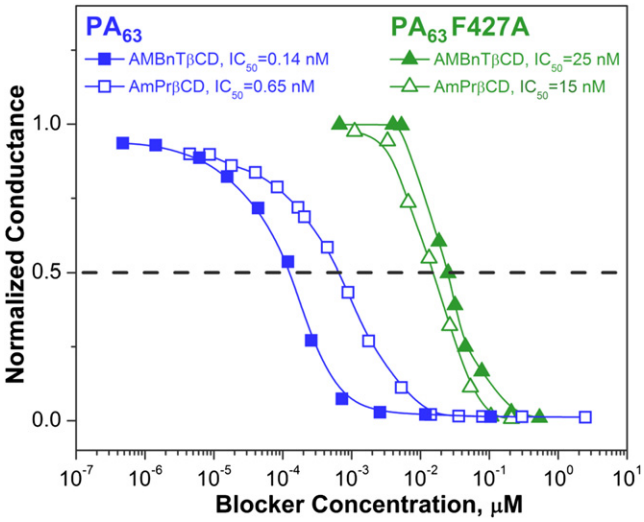

FIGURE 7 Deletion of the φ-clamp significantly decreases the efficacy of the blockers. The multichannel conductances of WT PA_{63} (*two curves on the left*) and the F427A mutant of PA_{63} (*two curves on the right*) are inhibited by AmPrβCD (*open symbols*) and AMBnTβCD (*filled symbols*) blockers, with the IC_{50} values differing by orders of magnitude. Membranes were bathed by 0.1 M KCl solution at pH 6, and the applied voltage was 20 mV.

Whatever the reason for the similarity in the blockage voltage sensitivity, the expressed voltage dependence itself points toward the blocker charge interaction with the applied transmembrane field as an important component of blockage regulation. In addition, the data in Fig. 6 suggest that there is another long-range electrostatic component, $\Delta U_C([C])$, which is most pronounced at small salt concentrations $[C]$. To dissect the blocker-channel interaction into different quantifiable components, we will use the framework of a simple model of solute dynamics in the channel (47). We will assume that the total interaction can be characterized by a rectangular potential well of depth $\Delta U(V,[C])$ occupying the entire blocker-accessible cylindrical part of the pore:

$$\Delta U(V,[C]) = \Delta U_C([C]) + \delta zeV + \Delta U_{SR}, \qquad (1)$$

where ze is the blocker charge, δ is the dimensionless apparent electrical distance, and V is the applied voltage. Here the second term represents the blocker interaction with the transmembrane field and ΔU_{SR} is the salt-concentration-independent, short-range component of interaction manifested by the saturating parts of the dependencies in Fig. 6. In this analysis, we will ignore the weak dependence of the on-rate on salt concentration and voltage, and consider it constant. Then, for a deep potential well, the residence time of the blocker molecule in the channel as a function of the applied voltage and salt concentration can be written as

$$\tau_{off}(V,[C]) = \frac{1}{\nu}\exp\left(\frac{\Delta U_C([C]) + \delta zeV + \Delta U_{SR}}{k_B T}\right), \qquad (2)$$

where k_B is the Boltzmann constant, T is the absolute temperature, and $1/\nu$ is a prefactor determined by a number of parameters, such as the difference in the radii of the blocker and the blocker-accessible part of the pore, the length of the pore, and the diffusion coefficient of the blocker (48).

From Eq. 2, for a constant applied voltage we have

$$\tau_{off}([C]) = \tau_0 \exp\left(\frac{\Delta U_C([C])}{k_B T}\right), \qquad (3)$$

where τ_0 is the salt-concentration-independent residence time. To crudely evaluate the salt-concentration-dependent contribution, as a possible candidate we consider Coulomb interaction between the fixed charges on the walls of the pores Q_p and the seven elementary charges on the blocker molecule. In bulk water, an estimate for the energy of this interaction can be written as a function of salt concentration and distance r between the charges as

$$\Delta U_C([C]) = \frac{1}{4\pi\,\varepsilon\varepsilon_0}\,\frac{zeQ_p}{r}\exp\left(-\frac{r}{\lambda_D([C])}\right), \qquad (4)$$

where ε_0 is the dielectric constant of vacuum, ε is a ratio of the dielectric constant of water to that of vacuum, and $\lambda_D([C])$ is the concentration-dependent Debye length.

The solid lines in Fig. 6 give the best fits of Eq. 4 with $z = 7$ to the experimental data obtained for the two blockers and three channels. The effective charge of the channel pore Q_p was used as a fitting parameter for each of the six systems, and distance r was chosen as 1.2 nm for all of the systems. The results in the case of the AmPrβCD blocker are as follows: $Q_p = 8.2\ e$ for the PA_{63} pore, $Q_p = 5.9\ e$ for the C2IIa pore, and $Q_p = 2.2\ e$ for the Ib pore, showing the decreased pore charge in the sequence. This finding qualitatively agrees with the predictions based on the data for the conductance salt dependence and selectivity of the three channels (17,22,41,42). For the more-effective blocker, AMBnTβCD, the salt-independent interactions are more pronounced. The Coulomb component is now described by the set of the following effective charges: $Q_p = 4.9\ e$ for the PA_{63} pore, $Q_p = 4.2\ e$ for the C2IIa pore, and $Q_p = 3.4\ e$ for the Ib pore, showing the same sequence. Thus, the strongest Coulomb component, accounting for ~4 k_BT per molecule when salt concentration in the bulk is reduced from 2 M to 0.3 M KCl, is seen for the PA_{63} pore blockage with AmPrβCD.

Note that Eq. 4 gives only an extremely crude description of the salt-concentration-dependent component of the blocker-channel interaction. There are several main reasons for this. First, these equations hold true for a point charge interacting with another point charge, and not for the complex constellation of charges on the blocker molecule and on the channel protein. Second, they describe Coulomb interactions in water, and not in the highly inhomogeneous water/protein media of the channel lumen. Third, calculations of the total electrostatic energy should necessarily include solvation energies and energies associated with possible conformational changes (49). Nevertheless, even this simple description allows one to obtain a reasonable set of charge and distance parameters, and an acceptable dependence of the interaction on salt concentration, thus suggesting significant involvement of long-range electrostatics, especially at physiological salt conditions. The important role of long-range electrostatics was also demonstrated in a number of recent studies devoted to PA_{63} channel interactions with its substrates (26,50–57).

Estimation of the salt-concentration-independent part, ΔU_{SR}, is most difficult because it requires knowledge of the prefactor $1 / v$ in Eq. 2. Because the calculation of this prefactor requires detailed information about the structure and potential profile of the blocker-channel interaction (48), we will use an alternative consideration, namely, the partition coefficient. The partition coefficient, which is defined as a ratio of blocker concentration in the channel, $[C^{ch}_{\text{blocker}}]$, to its concentration in the bulk, $[C^{b}_{\text{blocker}}]$, can be written as

$$P(V,[C]) = \frac{[C^{ch}_{\text{blocker}}]}{[C^{b}_{\text{blocker}}]} = \exp\left[\frac{\Delta U(V,[C])}{k_BT}\right]. \quad (5)$$

Blocker concentration in the channel can be estimated based on the results of our previous study of AmPrβCD interaction with the anthrax pore (33) and structural predictions for the pore. The values of τ_{on} and τ_{off} taken from Fig. 3, *b* and *c*, of Nestorovich et al. (33) for 1 M KCl and $[C^{b}_{\text{blocker}}] = 3 \times 10^{-8}$ M allow us to calculate the pore occupancy at this blocker concentration as $\langle N\rangle = \tau_{off}/(\tau_{off} + \tau_{on}) \simeq 0.084$. From the structure of the blocker (Fig. 1) and the structural predictions of Katayama et al. (24), the channel volume available for the center of the blocker molecule can be evaluated as $v \simeq 12\ \text{nm}^3$. This leads to the following estimate for blocker concentration in the channel: $\langle N\rangle / v \simeq 0.7 \times 10^{25}\ \text{m}^{-3}$ or $[C^{ch}_{\text{blocker}}] \simeq 1.2 \times 10^{-2}$ M. Then, using Eq. 5, we obtain $\Delta U(V,[C]) \simeq 13\ k_BT$ or ~8 kcal/mol. Indeed, this is a lower estimate for the depth of the potential well because the effective binding volume (58) of the blocker molecule can be much smaller than the volume evaluated from the structural prediction used here.

Although recent research demonstrated that interactions between cyclodextrins and protein nanopores are remarkably sophisticated (59), our experiments with the F427A mutant of PA_{63} strongly suggest that a significant part of the salt-independent interactions described by ΔU_{SR} is coming from the blockers' interaction with the φ-clamp. Removal of the clamp reduces the blocker-channel interaction by ~2 kcal/mol for the AmPrβCD and by ~3 kcal/mol for the AMBnTβCD blocker. Note that mutations in the ϕ-clamp were previously shown to significantly affect the binding affinity of a number of compounds with both PA_{63} (25) and C2IIa channels (29), preferring aromatic moieties by 0.7 kcal/mol per aromatic ring (25).

The on-rates of the blockage given in Table 1 do not show any clear dependence on the applied voltage. The AMBnTβCD on-rate also did not exhibit dependence on salt concentration (data not shown). As we reported earlier (33), the AmPrβCD on-rate decreases by ~4-fold as salt concentration increases from 0.3 M KCl to 2.0 M KCl. When the on-rate data from Fig. 6 *B* of Nestorovich et al. (33) are replotted as a function of salt activity, they demonstrate a good linear regression that can be characterized by the osmotic sensitivity of −29 water molecules (60), suggesting that the mechanism of this salt dependence is the preferential solvation of AmPrβCD in the bulk by salt ions. More importantly, the data in Table 1 given for 1 M KCl solutions do not reveal any statistically significant difference between the on-rate constants for the two blockers. Averaging the on-rates measured for the three channels and three voltages, we obtain the following values: $k_{on} = (2.9 \pm 1.1) \times 10^7\ (\text{M}\cdot\text{s})^{-1}$ for AmPrβCD, and $k_{on} = (2.6 \pm 1.2) \times 10^7\ (\text{M}\cdot\text{s})^{-1}$ for the much more efficient AMBnTβCD. This allows us to conclude that the most important interactions

determining blocker efficiency are interactions between the blocker molecule and the channel lumen analyzed above.

Thus, the blockage efficiency of the translocation pores of the three binary toxins depends on a number of parameters. In this study, we used rather high salt concentrations of ≥ 0.3 M because, in similarity to our findings with PA_{63} and AmPrβCD (33), at the decreasing KCl concentrations, all three channels started to display a supplementary mode of blocker action. In addition to the reversible blockage obeying a two-state Markov process, the presence of blockers enhanced the voltage gating of these channels, making their closed states more favorable. Together with the increasing contribution of Coulomb interactions, this supplementary mode further improved the efficiency of the blockers but made the quantitative analysis of the two process acting in parallel difficult due to problems with their separation. Among the studied channels, the blocker-enhanced gating was minimal for Ib and maximal for PA_{63}. According to our measurements on multichannel membranes, which do not discriminate between the two modes of action, for AMBnTβCD this resulted in $IC_{50} = (0.13 \pm 0.1)$ nM for PA_{63}, $IC_{50} = (1.5 \pm 0.5)$ nM for C2IIa, and $IC_{50} = (23 \pm 10)$ nM for Ib channels at "physiological" 0.1 M KCl.

CONCLUDING REMARKS

A better understanding of the physical forces that are responsible for the pore-blocker interaction is imperative for the directed chemical synthesis of effective blockers with broad-spectrum activity against pore-forming bacterial toxins. Analysis of the dependence of the interaction strength and underlying kinetics on the salt concentration, the applied potential, and, in the case of the PA_{63} pore, the presence of the φ-clamp, allows one to identify at least three components:

1. The residence time at high salt concentrations interpolated to zero voltage allows an estimation of salt-concentration-independent, short-range interactions, which predominate in all six cases studied. In the case of AMBnTβCD, its binding to the PA_{63}, C2IIa, and Ib pores is further enhanced by the presence of aromatic groups most probably interacting with the φ-clamp (25) in the lumen of these channels. This conclusion is supported by the F427A mutation of PA_{63}, which not only reduces the binding constants by more than an order of magnitude but makes the blockage by AmPrβCD and AMBnTβCD indistinguishable, thus abolishing the effect of addition of the aromatic groups.
2. The dependence of the blockers' residence times on salt concentration reveals the contribution of long-range Coulomb interactions at moderate and low salt concentrations. At physiological salt concentrations, Coulomb interactions increase the binding efficiency by orders of magnitude. At salt concentrations < 0.5 M, the AmPrβCD residence time increases in the order Ib $<$ C2IIa $<$ PA_{63}, and so does the cationic selectivity of the channels. This pattern is Ib $\approx$ C2IIa $<$ PA_{63} for the AMBnTβCD binding. The difference in the affinity of positively charged blockers toward the PA_{63}, C2IIa, and Ib channels was previously attributed to the different number of negatively charged amino acids on the lumen of these pores (22,29,42).
3. The increase in the blockers' residence times with the applied voltage demonstrates the existence of an additional electrostatic component of the interaction. Usually, the residence time dependence on the applied voltage allows for an estimation of the depth of the blocker penetration into the pore, but this may not be the case for the mesoscopic channels studied here. Nevertheless, the interaction of the charges with the transmembrane electric field is an additional factor in regulating the blocker efficacy.

We thank Tanisha Robinson, Rasem Fattah, and Clinton E. Leysath for excellent technical assistance. E.M.N. thanks Dr. Philip Gurnev (Eunice Kennedy Shriver National Institute of Child Health and Human Development, National Institutes of Health) for his help in setting up her laboratory.

This study was supported by the Intramural Research Programs of the National Institutes of Health, the Eunice Kennedy Shriver National Institute of Child Health and Human Development, and the National Institute of Allergy and Infectious Diseases, and by startup funds from The Catholic University of America. V.A.K. is an employee and shareholder of Innovative Biologics.

REFERENCES

1. Barth, H., K. Aktories, …, B. G. Stiles. 2004. Binary bacterial toxins: biochemistry, biology, and applications of common *Clostridium* and *Bacillus* proteins. *Microbiol. Mol. Biol. Rev.* 68:373–402.
2. Barth, H., and B. G. Stiles. 2008. Binary actin-ADP-ribosylating toxins and their use as molecular Trojan horses for drug delivery into eukaryotic cells. *Curr. Med. Chem.* 15:459–469.
3. Collier, R. J. 2009. Membrane translocation by anthrax toxin. *Mol. Aspects Med.* 30:413–422.
4. Sakurai, J., M. Nagahama, …, K. Kobayashi. 2009. *Clostridium perfringens* iota-toxin: structure and function. *Toxins (Basel).* 1:208–228.
5. Barth, H., D. Blocker, …, K. Aktories. 2000. Cellular uptake of *Clostridium botulinum* C2 toxin requires oligomerization and acidification. *J. Biol. Chem.* 275:18704–18711.
6. Petosa, C., R. J. Collier, …, R. C. Liddington. 1997. Crystal structure of the anthrax toxin protective antigen. *Nature.* 385:833–838.
7. Kintzer, A. F., K. L. Thoren, …, B. A. Krantz. 2009. The protective antigen component of anthrax toxin forms functional octameric complexes. *J. Mol. Biol.* 392:614–629.
8. Singh, Y., K. R. Klimpel, …, S. H. Leppla. 1994. The chymotrypsin-sensitive site, FFD315, in anthrax toxin protective antigen is required for translocation of lethal factor. *J. Biol. Chem.* 269:29039–29046.
9. Cunningham, K., D. B. Lacy, …, R. J. Collier. 2002. Mapping the lethal factor and edema factor binding sites on oligomeric anthrax protective antigen. *Proc. Natl. Acad. Sci. USA.* 99:7049–7053.
10. Milne, J. C., D. Furlong, …, R. J. Collier. 1994. Anthrax protective antigen forms oligomers during intoxication of mammalian cells. *J. Biol. Chem.* 269:20607–20612.

11. Mogridge, J., M. Mourez, and R. J. Collier. 2001. Involvement of domain 3 in oligomerization by the protective antigen moiety of anthrax toxin. *J. Bacteriol.* 183:2111–2116.
12. Abrami, L., S. Liu, …, F. G. van der Goot. 2003. Anthrax toxin triggers endocytosis of its receptor via a lipid raft-mediated clathrin-dependent process. *J. Cell Biol.* 160:321–328.
13. Nagahama, M., T. Hagiyama, …, J. Sakurai. 2009. Binding and internalization of *Clostridium botulinum* C2 toxin. *Infect. Immun.* 77:5139–5148.
14. Pust, S., H. Barth, and K. Sandvig. 2010. *Clostridium botulinum* C2 toxin is internalized by clathrin- and Rho-dependent mechanisms. *Cell. Microbiol.* 12:1809–1820.
15. Blöcker, D., J. Behlke, …, H. Barth. 2001. Cellular uptake of the *Clostridium perfringens* binary iota-toxin. *Infect. Immun.* 69:2980–2987.
16. Stiles, B. G., M. L. Hale, …, M. R. Popoff. 2002. *Clostridium perfringens* iota toxin: characterization of the cell-associated iota b complex. *Biochem. J.* 367:801–808.
17. Schmid, A., R. Benz, …, K. Aktories. 1994. Interaction of *Clostridium botulinum* C2 toxin with lipid bilayer membranes. Formation of cation-selective channels and inhibition of channel function by chloroquine. *J. Biol. Chem.* 269:16706–16711.
18. Bachmeyer, C., R. Benz, …, M. R. Popoff. 2001. Interaction of *Clostridium botulinum* C2 toxin with lipid bilayer membranes and Vero cells: inhibition of channel function by chloroquine and related compounds in vitro and intoxification in vivo. *FASEB J.* 15:1658–1660.
19. Blöcker, D., K. Pohlmann, …, H. Barth. 2003. *Clostridium botulinum* C2 toxin: low pH-induced pore formation is required for translocation of the enzyme component C2I into the cytosol of host cells. *J. Biol. Chem.* 278:37360–37367.
20. Blöcker, D., C. Bachmeyer, …, H. Barth. 2003. Channel formation by the binding component of *Clostridium botulinum* C2 toxin: glutamate 307 of C2II affects channel properties in vitro and pH-dependent C2I translocation in vivo. *Biochemistry.* 42:5368–5377.
21. Gibert, M., J. C. Marvaud, …, M. R. Popoff. 2007. Differential requirement for the translocation of clostridial binary toxins: iota toxin requires a membrane potential gradient. *FEBS Lett.* 581:1287–1296.
22. Knapp, O., R. Benz, …, M. R. Popoff. 2002. Interaction of *Clostridium perfringens* iota-toxin with lipid bilayer membranes. Demonstration of channel formation by the activated binding component Ib and channel block by the enzyme component Ia. *J. Biol. Chem.* 277:6143–6152.
23. Blaustein, R. O., T. M. Koehler, …, A. Finkelstein. 1989. Anthrax toxin: channel-forming activity of protective antigen in planar phospholipid bilayers. *Proc. Natl. Acad. Sci. USA.* 86:2209–2213.
24. Katayama, H., B. E. Janowiak, …, M. T. Fisher. 2008. GroEL as a molecular scaffold for structural analysis of the anthrax toxin pore. *Nat. Struct. Mol. Biol.* 15:754–760.
25. Krantz, B. A., R. A. Melnyk, …, R. J. Collier. 2005. A phenylalanine clamp catalyzes protein translocation through the anthrax toxin pore. *Science.* 309:777–781.
26. Krantz, B. A., A. Finkelstein, and R. J. Collier. 2006. Protein translocation through the anthrax toxin transmembrane pore is driven by a proton gradient. *J. Mol. Biol.* 355:968–979.
27. Melnyk, R. A., and R. J. Collier. 2006. A loop network within the anthrax toxin pore positions the phenylalanine clamp in an active conformation. *Proc. Natl. Acad. Sci. USA.* 103:9802–9807.
28. Lang, A. E., T. Neumeyer, …, K. Aktories. 2008. Amino acid residues involved in membrane insertion and pore formation of *Clostridium botulinum* C2 toxin. *Biochemistry.* 47:8406–8413.
29. Neumeyer, T., B. Schiffler, …, R. Benz. 2008. *Clostridium botulinum* C2 toxin. Identification of the binding site for chloroquine and related compounds and influence of the binding site on properties of the C2II channel. *J. Biol. Chem.* 283:3904–3914.
30. Karginov, V. A., E. M. Nestorovich, …, S. M. Bezrukov. 2005. Blocking anthrax lethal toxin at the protective antigen channel by using structure-inspired drug design. *Proc. Natl. Acad. Sci. USA.* 102: 15075–15080.
31. Karginov, V. A., E. M. Nestorovich, …, S. M. Bezrukov. 2006. Search for cyclodextrin-based inhibitors of anthrax toxins: synthesis, structural features, and relative activities. *Antimicrob. Agents Chemother.* 50: 3740–3753.
32. Karginov, V. A., E. M. Nestorovich, …, S. M. Hecht. 2007. Inhibition of *S. aureus* α-hemolysin and *B. anthracis* lethal toxin by β-cyclodextrin derivatives. *Bioorg. Med. Chem.* 15:5424–5431.
33. Nestorovich, E. M., V. A. Karginov, …, S. M. Bezrukov. 2010. Blockage of anthrax PA_{63} pore by a multicharged high-affinity toxin inhibitor. *Biophys. J.* 99:134–143.
34. Nestorovich, E. M., V. A. Karginov, …, H. Barth. 2011. Tailored β-cyclodextrin blocks the translocation pores of binary exotoxins from *C. botulinum* and *C. perfringens* and protects cells from intoxication. *PLoS ONE.* 6:e23927.
35. Moayeri, M., T. M. Robinson, …, V. A. Karginov. 2008. In vivo efficacy of β-cyclodextrin derivatives against anthrax lethal toxin. *Antimicrob. Agents Chemother.* 52:2239–2241.
36. Barth, H., J. C. Preiss, …, K. Aktories. 1998. Characterization of the catalytic site of the ADP-ribosyltransferase *Clostridium botulinum* C2 toxin by site-directed mutagenesis. *J. Biol. Chem.* 273:29506–29511.
37. Perelle, S., M. Domenighini, and M. R. Popoff. 1996. Evidence that Arg-295, Glu-378, and Glu-380 are active-site residues of the ADP-ribosyltransferase activity of iota toxin. *FEBS Lett.* 395:191–194.
38. Pomerantsev, A. P., O. M. Pomerantseva, …, S. H. Leppla. 2011. A *Bacillus anthracis* strain deleted for six proteases serves as an effective host for production of recombinant proteins. *Protein Expr. Purif.* 80: 80–90.
39. Montal, M., and P. Mueller. 1972. Formation of bimolecular membranes from lipid monolayers and a study of their electrical properties. *Proc. Natl. Acad. Sci. USA.* 69:3561–3566.
40. Bachmeyer, C., F. Orlik, …, R. Benz. 2003. Mechanism of C2-toxin inhibition by fluphenazine and related compounds: investigation of their binding kinetics to the C2II-channel using the current noise analysis. *J. Mol. Biol.* 333:527–540.
41. Blaustein, R. O., E. J. Lea, and A. Finkelstein. 1990. Voltage-dependent block of anthrax toxin channels in planar phospholipid bilayer membranes by symmetric tetraalkylammonium ions. Single-channel analysis. *J. Gen. Physiol.* 96:921–942.
42. Orlik, F., B. Schiffler, and R. Benz. 2005. Anthrax toxin protective antigen: inhibition of channel function by chloroquine and related compounds and study of binding kinetics using the current noise analysis. *Biophys. J.* 88:1715–1724.
43. Bezrukov, S. M., and M. Winterhalter. 2000. Examining noise sources at the single-molecule level: 1/f noise of an open maltoporin channel. *Phys. Rev. Lett.* 85:202–205.
44. French, R. J., and J. J. Shoukimas. 1985. An ion's view of the potassium channel. The structure of the permeation pathway as sensed by a variety of blocking ions. *J. Gen. Physiol.* 85:669–698.
45. Woodhull, A. M. 1973. Ionic blockage of sodium channels in nerve. *J. Gen. Physiol.* 61:687–708.
46. Strichartz, G. R. 1973. The inhibition of sodium currents in myelinated nerve by quaternary derivatives of lidocaine. *J. Gen. Physiol.* 62:37–57.
47. Bezrukov, S. M., A. M. Berezhkovskii, and A. Szabo. 2007. Diffusion model of solute dynamics in a membrane channel: mapping onto the two-site model and optimizing the flux. *J. Chem. Phys.* 127:115101.
48. Berezhkovskii, A. M., M. A. Pustovoit, and S. M. Bezrukov. 2003. Channel-facilitated membrane transport: average lifetimes in the channel. *J. Chem. Phys.* 119:3943–3951.
49. Gilson, M. K., and B. Honig. 1988. Calculation of the total electrostatic energy of a macromolecular system: solvation energies, binding energies, and conformational analysis. *Proteins.* 4:7–18.
50. Pentelute, B. L., A. P. Barker, …, R. J. Collier. 2010. A semisynthesis platform for investigating structure-function relationships in the N-terminal domain of the anthrax Lethal Factor. *ACS Chem. Biol.* 5:359–364.

51. Pentelute, B. L., O. Sharma, and R. J. Collier. 2011. Chemical dissection of protein translocation through the anthrax toxin pore. *Angew. Chem. Int. Ed. Engl.* 50:2294–2296.

52. Basilio, D., S. J. Juris, …, A. Finkelstein. 2009. Evidence for a proton-protein symport mechanism in the anthrax toxin channel. *J. Gen. Physiol.* 133:307–314.

53. Basilio, D., P. K. Kienker, …, A. Finkelstein. 2011. A kinetic analysis of protein transport through the anthrax toxin channel. *J. Gen. Physiol.* 137:521–531.

54. Basilio, D., L. D. Jennings-Antipov, …, A. Finkelstein. 2011. Trapping a translocating protein within the anthrax toxin channel: implications for the secondary structure of permeating proteins. *J. Gen. Physiol.* 137:343–356.

55. Thoren, K. L., E. J. Worden, …, B. A. Krantz. 2009. Lethal factor unfolding is the most force-dependent step of anthrax toxin translocation. *Proc. Natl. Acad. Sci. USA.* 106:21555–21560.

56. Brown, M. J., K. L. Thoren, and B. A. Krantz. 2011. Charge requirements for proton gradient-driven translocation of anthrax toxin. *J. Biol. Chem.* 286:23189–23199.

57. Janowiak, B. E., A. Fischer, and R. J. Collier. 2010. Effects of introducing a single charged residue into the phenylalanine clamp of multimeric anthrax protective antigen. *J. Biol. Chem.* 285:8130–8137.

58. Gilson, M. K., J. A. Given, …, J. A. McCammon. 1997. The statistical-thermodynamic basis for computation of binding affinities: a critical review. *Biophys. J.* 72:1047–1069.

59. Banerjee, A., E. Mikhailova, …, H. Bayley. 2010. Molecular bases of cyclodextrin adapter interactions with engineered protein nanopores. *Proc. Natl. Acad. Sci. USA.* 107:8165–8170.

60. Gurnev, P. A., D. Harries, …, S. M. Bezrukov. 2010. Osmotic stress regulates the strength and kinetics of sugar binding to the maltoporin channel. *J. Phys. Condens. Matter.* 22:454110.